CYTOMETRY
Journal of Quantitative Cell Science PART A

Evaluating spectral cytometry for immune profiling in viral disease

Paula Niewold,[1†] Thomas Myles Ashhurst,[2†] Adrian Lloyd Smith,[2] Nicholas Jonathan Cole King[1,2*]

[1]Discipline of Pathology, Charles Perkins Centre, The Faculty of Medicine and Health, Camperdown, New South Wales, Australia

[2]Sydney Cytometry Core Research Facility, Charles Perkins Centre, The Centenary Institute and The University of Sydney, Johns Hopkins Drive, Camperdown, New South Wales, Australia

Received 4 November 2019; Revised 23 June 2020; Accepted 25 June 2020

Grant sponsor: International Society for the Advancement of Cytometry (ISAC), Grant number Marylou Ingram Scholars Program; Grant sponsor: Merridew Foundation; Grant sponsor: National Health and Medical Research Council, Grant number: 1088242

Additional Supporting Information may be found in the online version of this article.

*Correspondence to: Nicholas Jonathan Cole King, Charles Perkins Centre, D17, Johns Hopkins Dr, University of Sydney, Camperdown, NSW 2050, Australia
Email: nicholas.king@sydney.edu.au

†These authors contributed equally to this work.

Published online in Wiley Online Library (wileyonlinelibrary.com)

DOI: 10.1002/cyto.a.24211

Abstract

In conventional fluorescence cytometry, each fluorophore present in a panel is measured in a target detector, through the use of wide band-pass optical filters. In contrast, spectral cytometry uses a large number of detectors with narrow band-pass filters to measure a fluorophore's signal across the spectrum, creating a more detailed fluorescent signature for each fluorophore. The spectral approach shows promise in adding flexibility to panel design and improving the measurement of fluorescent signal. However, few comparisons between conventional and spectral systems have been reported to date. We therefore sought to compare a modern conventional cytometry system with a modern spectral system, and to assess the quality of resulting datasets from the point of view of a flow cytometry user. Signal intensity, spread, and resolution were compared between the systems. Subsequently, the different methods of separating fluorophore signals were compared, where compensation mathematically separates multiple overlapping fluorophores and unmixing relies on creating a detailed fluorescent signature across the spectrum to separate the fluorophores. Within the spectral data set, signal spread and resolution were comparable between compensation and unmixing. However, for some highly overlapping fluorophores, unmixing resolved the two fluorescence signals where compensation did not. Finally, data from mid- to large-size panels were acquired and were found to have comparable resolution for many fluorophores on both instruments, but reduced levels of spreading error on our spectral system improved signal resolution for a number of fluorophores, compared with our conventional system. Furthermore, autofluorescence extraction on the spectral system allowed for greater population resolution in highly autofluorescent samples. Overall, the implementation of a spectral cytometry approach resulted in data that are comparable to that generated on conventional systems, with a number of potential advantages afforded by the larger number of detectors, and the integration of the spectral unmixing approach.

Key terms

spectral cytometry; unmixing; compensation; high-dimensional; polychromatic; viral encephalitis

Introduction

Fluorescence Cytometry and Spreading Error

Flow cytometry is a technique that utilizes the emission of multiple fluorescently labeled antibodies excited by a laser to measure the simultaneous expression of various proteins on single cells. The high sensitivity and high-throughput nature of this technique, in conjunction with the increasing numbers of available fluorophore labels, make it suitable for the characterization of many cell subsets under a wide variety of conditions. In conventional cytometry, individual detectors (often photomultiplier tubes [PMTs]) are used to record the signal from specific target fluorophores following excitation with a laser (Fig. 1A) via selective optical filters

with wide band-pass properties, to maximize the amount of light collected (Fig. 1B). As such, each detector is effectively tailored to a particular fluorophore, restricting the range of fluorophores that can be used on these systems, thus limiting reagent flexibility. Many fluorophores that are used simultaneously may have overlapping emission spectra, leading to spillover of one fluorophore into a nontarget detector (Fig. 1C,D). However, the process of compensation can mathematically correct for the overlap of signal from a target fluorophore into all other nontarget detectors (Fig. 1E) (1, 2). Through the application of linear algebra, the spillover of each fluorophore into all detectors is corrected such that each detector effectively contains information for only a single dye. This is achieved by multiplying the measured signal in each detector by the inverse of a mixing matrix, scaled columns wise to 1 (3). Errors or uncertainty in photon counting complicates the correction of mixed signals resulting from spillover, as they are not described by a Gaussian distribution. Thus, applying a linear correction to the nonlinear counted photons results in an error in the distribution of the spillover fluorophore signal in nontarget detectors. This is referred to as spreading error (SE) (4). It manifests as an increased width of the signal from a spillover fluorophore in a nontarget detector after compensation, and the spread of this signal increases as the fluorescence intensity of the spillover fluorophore increases. Importantly, compensation does not introduce this error, but rather the process of compensation moves the signal distribution to the low end of a logarithmic or bi-exponential/Logicle scale. As a result, this signal distribution appears to expand. SE can complicate separating the negative and positive populations that are being measured in that detector. The construction of high-quality panels requires careful panel design to reduce the intensity of signals that have a large degree of SE, as not all fluorophores will exhibit the same level of SE in all detectors. Recently, advances in instrumentation and dye development have led to the development of panels that can incorporate more than 25 fluorophores simultaneously across five or more excitation lasers (5-7), with reports of 40-color panels beginning to emerge.

Spectral Cytometry

An alternative approach to measuring multiple overlapping fluorophores on single cells is through the use of spectral cytometry. The use of spectral approaches for flow cytometry was demonstrated as early as 2004 by Robinson et al. (8, 9), resulting in a patent (10) and its subsequent licensing to Sony for a commercial spectral flow cytometer (11). Since then, a number of studies have demonstrated the utility of the spectral approach in various flow cytometry experiments (11-16) including the use of panels with more than 20 colors (16), with 40 colors on a spectral system recently reported (17). This technique aims to measure as much of the whole emission spectrum of a fluorophore as possible, across a large number of detectors with narrow band-pass properties, rather than the peak emission in a single detector with wide band-pass properties. Additionally, differential excitation of fluorophores by multiple lasers further increases the granularity of this spectral signature. This design allows for the measurement of any fluorophore that is sufficiently excited by the lasers in use, avoiding the fluorophore-specific detector design characteristic of conventional systems. The signals measured across multiple detectors (Fig. 1F–I) create a detailed fluorescence "signature" for each fluorophore, allowing each of these unique fluorescent signatures to be "unmixed" from one another. Key to this approach is the use of a large number of detectors on each laser line, more than are utilized in conventional systems (Fig. 1J,K). This process potentially allows fluorophores with similar emission properties, which would normally be measured in the same detector on a conventional system, to be measured simultaneously on a spectral system and separated using conventional compensation approaches, or through unmixing based on their differential spectral signatures (Fig. 1L,M). In addition, using this approach, a signature can be determined for cellular autofluorescence in individual samples, allowing for the unmixing of autofluorescence from affected channels, as well as the measurement of autofluorescence as an additional feature. Taken together, the large number of incorporated detectors, the spectral unmixing approach, and the detailed signatures generated for each fluorophore enables the building of large and flexible fluorescent panels that are capable of incorporating highly overlapping dyes.

In conventional compensation, the correction of signal measured in all nontarget detectors is achieved through the inversion of a mixing matrix. In other fields, such as remote sensing and spectral microscopy, various methods of spectral unmixing are applied (18). The unmixing approach used in the spectral system we tested deploys a least-squares linear unmixing calculation. This approach assumes a linear contribution of reference spectra to a mixed signal, where unmixing is achieved through the application of matrix pseudo-inversion. This approach is very similar to compensation (inversion), where the number of columns and rows are the same, where one fluorophore is assigned per detector, but in spectral unmixing (pseudo-inversion), the number of detectors is larger than the number of fluorophores, potentially making the inversion more accurate. The object of this approach is to deconstruct mixed fluorescent signals into separate components (i.e., each individual fluorescent signal), so that the origin of a photon can be reassigned statistically to the source fluorophore (13). This is not the only method of unmixing available, and some approaches may be more suitable when the individual reference spectra are not known. Various comparisons of these approaches have been made elsewhere (13, 19).

Objectives of the Study

In this study, we sought to compare the performance of a conventional and a spectral cytometry system, specifically in signal quality, extent of spreading error, and signal resolution from spread for mid- to large-size panels, in a number of immunological contexts. Additionally, we sought to compare the results of compensation and unmixing when applied to

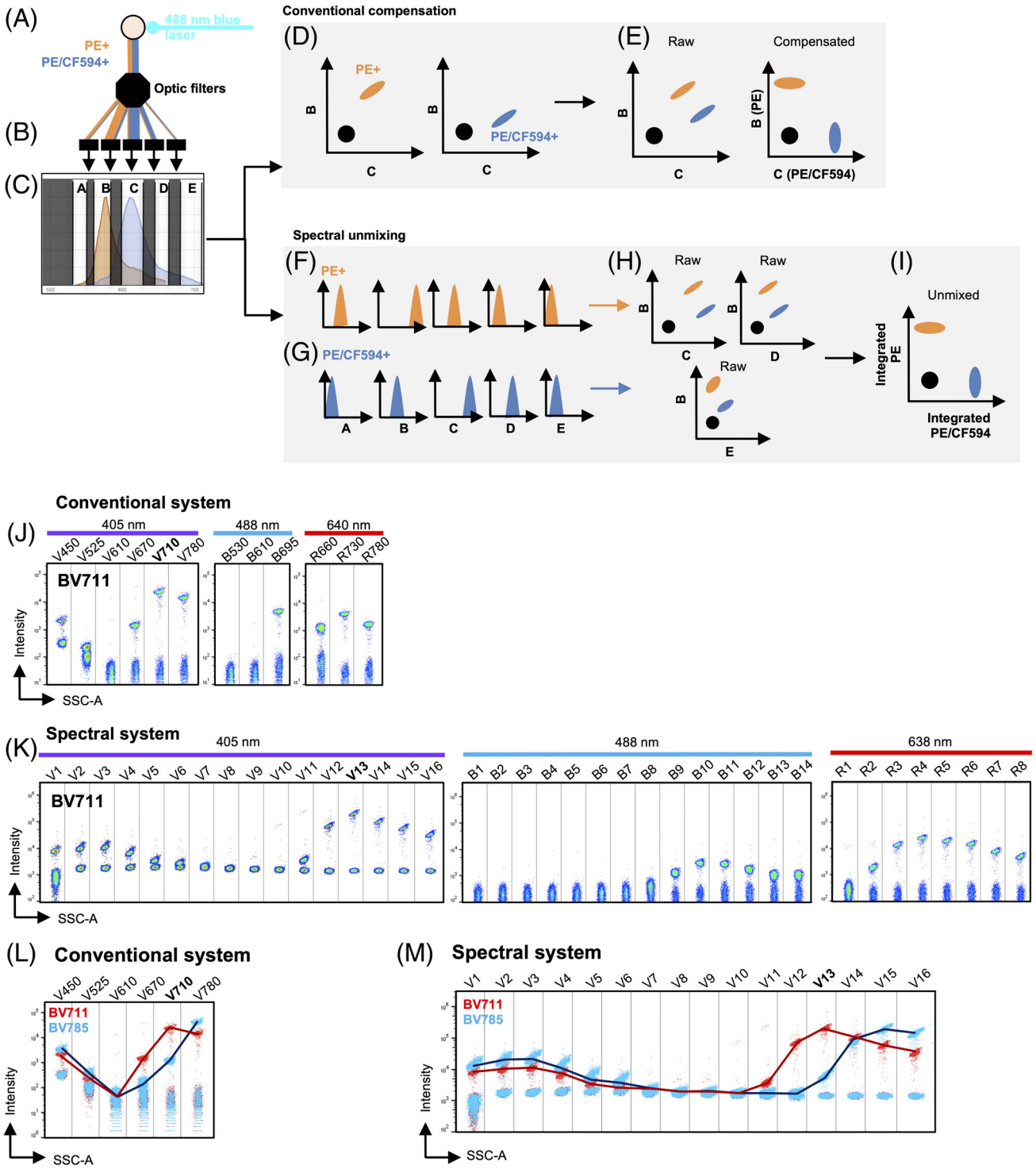

Figure 1. Conventional and spectral cytometry. A diagrammatic representation of conventional and spectral cytometry. In this example, (**A**) a blue 488 nm laser excites two fluorophores, PE and PE/CF594. (**B**) The emitted signal from both fluorophores is collected through optical filters, (**C**) and the relative signal arriving at each detector is shown. (**D**) Uncompensated raw data can then (**E**) be compensated to resolve the two signals. In spectral unmixing (**F** and **G**) signals are collected across a number of detectors, and (**H**) integrated signals are then unmixed from each other to generate (**I**) resolved signals. Compensation beads stained with BV711 plotted after acquisition (**J**) the conventional system and (**K**) spectral system. Profile of compensation beads stained with BV711 or BV785 when run on the (**L**) conventional or (**M**) spectral system, showing violet (405 nm) laser detectors only.

the data from the spectral system, to identify potential advantages of the spectral unmixing approach. Importantly, in comparing these systems, there are numerous differences in fluidics and optical design, and these designs do not necessarily reflect all conventional or spectral systems. As such, our aim was to assess these factors from the point of a view of a researcher applying flow cytometry experimentally, weighing the relative strengths and weaknesses in a research context, rather than providing a theoretical or mathematical comparison between the methods.

Methods

Mice and Anesthetics

Unless stated otherwise, all experiments were performed using female C57BL/6 mice aged between 8 and 12 weeks. Mice were purchased from the Animal Resources Centre (WA, Australia). All mice were housed (six per cage) in Hepa-filter cages with food and water supplied ad libitum as per the University of Sydney animal housing regulations. Ethical approval for the experimental use of mice was obtained from the Animal Ethics Committee at the University of Sydney, under protocols K20/8-2008/3/4863, K20/6-2012/3/5761, K20/11-2011/3/5660, and 2013/5660-273. Mice undergoing temporary anesthesia for intranasal inoculation, or other procedures, were injected *i.p.* with 250–300 ml of Avertin according to a weigh–volume nomogram. Mice undergoing terminal procedures were given 350–500 µl of anesthetic, followed by vena caval section and left ventricular cardiac perfusion with 30 ml of ice-cold PBS. Avertin anesthetic was prepared by dissolving 1 g of 2,2,2-tribromoethanol (Sigma-Aldrich) in 1 ml 2-methyl-2 butanol (Sigma-Aldrich). Heated tap water (50 ml) was then added to the solution and thoroughly mixed before sterilizing through a 0.2 mm syringe filter in 5 ml aliquots. The Avertin mixture was stored at −20°C in the dark until use.

Inoculation of Mice with West Nile Virus

Supine, anesthetized mice were inoculated intranasally with 10 µl of West Nile virus (WNV), 5 µl per nostril. Mice were given a total of 6×10^4 plaque-forming units (PFU), the lethal dose for 100% (LD_{100}) of mice by this route of inoculation.

Cell Isolation and Preparation

Bone marrow was prepared as described in reference (20). Mouse femurs were collected, and the distal and proximal ends removed with a scalpel or surgical scissors. The femur was then flushed with 1–3 ml of cold PBS (from a 5 ml syringe using a 33G needle) to collect BM cells into a 5 ml or 15 ml tube. Cells were then centrifuged at 500*g* for 5 min at 4°C to pellet the cells. Samples were then resuspended in 700 µl to 1 ml of fluorescence-activated cell sorting (FACS) buffer (PBS, 5 mM EDTA, 5% FCS), counted, and the desired cell numbers transferred to a 96-well plate for staining. Samples were kept on ice until antibody labeling later on the same day.

Spleens were removed from the peritoneal cavity and gently mashed through 70 µm cell strainers in 5 ml of cold PBS and centrifuged at 500*g* for 5 min at 4°C. Isolated spleen cells were then resuspended in 1–4 ml of FACS buffer and counted. After counting, cells were then placed in wells of a 96-well plate for cell staining. Samples were kept on ice until antibody labeling later on the same day.

Brain samples were prepared by cardiac perfusion with 30 ml of ice-cold PBS, under deep anesthesia to clear the blood vasculature. Brains were removed from the skull, and mechanically disrupted in cold PBS using a metal sieve. Brain homogenates were topped up to 18 ml of PBS and 2 ml of a 10X solution of deoxyribonuclease I (DNase I) and collagenase added for a final concentration of 1 mg/ml collagenase and 0.1 mg/ml DNase, and incubated at 37°C for 1 h. Alternatively, brains were placed into 9 ml of PBS in C-tubes (Miltenyi Biotech, Bergisch Gladbach, Germany), cut into eight sections, and kept at 4°C for up to 3 h on ice. Tubes then received 1 ml of 10X collagenase/DNase solution and the tissue was disrupted using a custom protocol on the GentleMacs auto-dissociator (Miltenyi Biotech, Bergisch Gladbach, Germany) for 30 min. Samples were then centrifuged (500*g*, 4°C, 10 min) and resuspended in 7 ml of a 30% Percoll solution (26.31% Percoll stock, 10% 1.5 M NaCl, 63.7% Media). This mixture was then slowly overlayed onto 3 ml of 80% Percoll (73.1% Percoll stock, 10% 1.5 M NaCl, 16.9% sterile H_2O) using a 10 ml pipette. The layered mixture was centrifuged at 1825*g* for 25 min at 25°C with the brake off. After centrifugation, the top layer of fat was removed and 2 ml of the cellular interface was pipetted into a new 15 ml tube and topped up with 5 ml FACS buffer, before centrifugation (500*g*, 4°C, 5 min) and resuspension in 250 µl of FACS buffer. Samples were kept on ice until flow cytometry antibody labeling later on the same day.

Cell suspensions from digested brain tissues were counted on a hemocytometer and assessed for viability using trypan blue exclusion. Bone marrow and spleen cell suspensions were analyzed on a XP-100 hematological analyzer (Sysmex, Kobe, Hyogo, Japan).

Cell Staining

Samples were distributed into wells of a 96-well plate, typically 1×10^6 cells per well, centrifuged at 300–500*g* for 5 min at 4°C and the supernatant discarded. Samples were then resuspended in 50 µl PBS-containing Zombie NIR Live/Dead (1/1,000, BioLegend, San Diego, CA) and purified anti-mouse CD16/32 (1/100, BioLegend), incubated for 20 min at 4°C, and then topped up with PBS before centrifugation. Samples were then resuspended in 50 µl of antibody master mix, and incubated for a further 30 min at 4°C before centrifugation and washed twice. Antibody details are provided in Supporting Information Table S4. Samples were then fixed in 4% paraformaldehyde (PFA) or fixation buffer (BioLegend) for 10 min. After fixation, samples not requiring intracellular staining were washed once, centrifuged at 800*g* for 5 min, and resuspended in FACS buffer and kept at 4°C for up to 3 days until flow cytometric acquisition. Alternatively, samples were

processed for intracellular staining. For instrument comparisons and compensation/unmixing, UltraComp beads (Thermo Fisher Scientific, Waltham, MA), or quantum simply cellular beads (QSCB) were labeled with selected fluorophore-conjugated antibodies in the same conditions as cellular samples, including staining time, temperature, and fixation.

Intracellular Staining

For intracellular staining of transcription factors, cells were washed in FACS buffer following fixation and permeabilized in 50–100 µl of FoxP3 fixation/permeabilization buffer (eBioscience, San Diego, CA) for 20 min at RT. After washing, samples were resuspended in 50 µl FoxP3 permeabilization buffer containing specific concentrations of intracellular antibodies. Samples were then incubated for 45 min at RT, washed in permeabilization buffer, and then washed in FACS buffer.

Instrumentation

For flow cytometry, samples were analyzed on a 4-laser Becton-Dickinson (BD, Franklin Lakes, NJ) Fortessa X-20 (conventional system), a 5-laser BD LSR-II (conventional system), or a 3-laser Cytek Aurora (spectral system). Configurations are provided in the Supporting Information Tables S1–S3. All instruments were subject to daily QC procedures before the samples were acquired. The data in Figures 1 and 2 were generated on the BD Fortessa X-20 (conventional system) or Cytek Aurora (spectral system). For these comparisons, only the violet, blue, and red lasers were used with fluorophores that were compatible with both systems. The data in Figures 4–7 were generated on the BD Fortessa X-20, BD LSR-II, or Cytek Aurora, as specified in the figure legends. The data in Figure 3 were generated on the spectral system only.

Data Analysis

For "peak channel" data, the channel with the peak signal for each fluorophore in each case was selected as the "target" detector, and compensation was performed in FlowJo v10.6.1 (BD). Of note, in the fluorochromes included in the study, each fluorophore peaked in a separate channel on the Aurora, as it has many more detectors than a conventional system; therefore, we did not need an approach to handle fluorochromes peaking in the same detector. Compensation for "virtual channel" data, and spectral unmixing, was performed in SpectroFlo software (Cytek Biosciences, Fremont, CA). Graphs were generated in PRISM (GraphPad, San Diego CA).

Results

Comparing Staining on the Conventional and Spectral System

Initially, we sought to compare the performance of a conventional and spectral system in terms of signal quality per fluorophore. To do this, we prepared compensation beads labeled with a variety of common fluorophores and recorded them on a conventional system (BD Fortessa X-20, using 12 detectors across 3 lasers) or a spectral system (Cytek Biosciences Aurora, Fremont, CA, using 38 detectors across 3 lasers). The spectral detectors allowed for measurement of fluorescence signal with a detection range up to at least 1×10^6, greater than the detection range up to 2.62×10^5 on the conventional system. For the fluorophore-bound beads analyzed in this experiment, the signal CVs were similar, suggesting similar signal quality (Supporting Information Fig. S1).

Comparing Signal Spread and Resolution on the Conventional and Spectral Systems

To compare data generated on each system in terms of signal spread and resolution, we examined the signal from pairs of fluorophore-labeled compensation beads, plotting the signal from fluorophores in neighboring detectors excited by the same laser (Fig. 2A–D) or from fluorophore pairs that exhibit similar emission properties excited by different lasers (Fig. 2E–H). For each fluorophore pair, the spread of the offending positive signal (red) is shown against the positive signal in the receiving detector (blue). We made these comparisons for compensated data from the conventional (Fig. 2A,E) and spectral systems when using data recorded in the peak channel (Fig. 2B,F). We also made these comparisons for compensated fluorophores on the spectral system after aggregating each signal into virtual filters (Fig. 2C,G), to match the filter configuration of the conventional system as closely as possible. Finally, we made these comparisons for data acquired on the spectral system after unmixing (Fig. 2D, H). To quantify these relationships, we used two metrics: a spreading ratio and a resolution ratio (Fig. 2I). The spreading ratio was calculated as the 99th percentile of the offending fluorophore in the receiving detector, divided by the 99th percentile of unstained beads in the same channel. The resolution ratio was calculated as the median of the receiving fluorophore in the receiving detector, divided by the 99th percentile of the offending fluorophore in the same detector. A demonstration of how these metrics reflect patterns on the plots is provided in the Supporting Information Figure S2.

When we compared compensated data from the conventional (Fig. 2A,E) and spectral system (peak detectors, Fig. 2B, F), higher levels of spread of the positive signal into neighboring or cross laser detectors (red arrows) were evident on the conventional system when compared to the spectral system. When we quantified this (Fig. 2J), we found that the degree of spread across all measured fluorophores was higher overall for the conventional system compared with the spectral system. However, because the signal intensity in the receiving detector (blue) was higher for the conventional system compared with the spectral system, the increased spread did not have a large impact on the resolution of signal from spread. When we quantified the resolution of the signal of the fluorophore in the receiving detector (blue) against the spreading signal (red), we found some cases where, despite decreased spread on the spectral system when compared to the conventional system, no change was found in the resolution of blue from red signal (e.g., PE-CF594 vs PerCP/Cy5.5). However, in

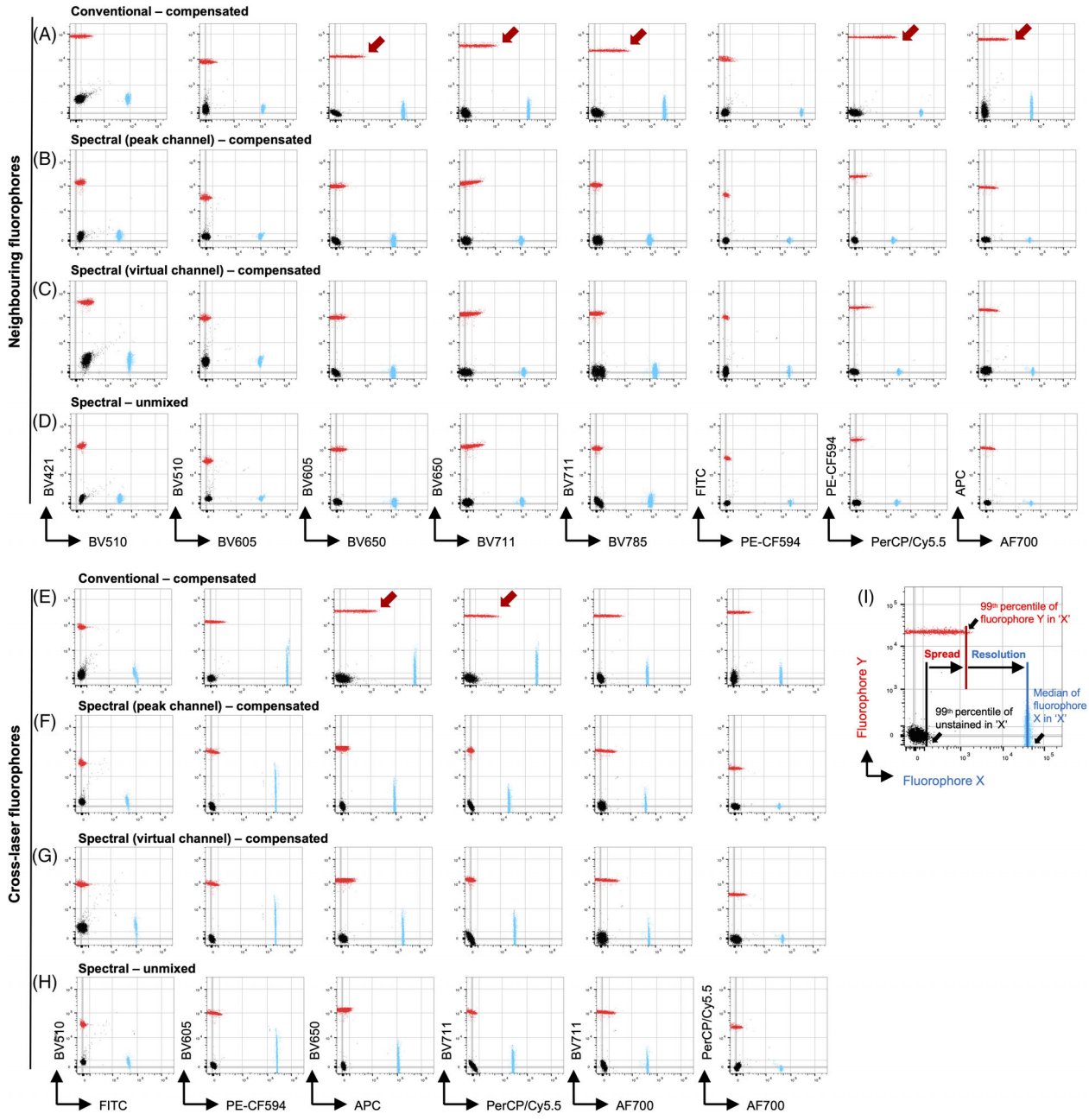

(J) **Signal spread**

		BV421/BV510	BV510/BV605	BV605/BV650	BV650/BV711	BV711/BV785	FITC/PECF594	PECF594/PerCPCy55	APC/AF700	BV510/FITC	BV605/PECF594	BV650/APC	BV711/PerCPCy55	BV711/AF700	PerCPCy55/AF700
Conventional	Compensated	0.95	2.92	9.54	12.10	8.58	2.35	17.67	8.49	0.76	3.01	6.83	5.96	6.95	4.56
Spectral (peak channels)	Compensated	0.75	1.16	2.15	3.18	0.84	1.12	4.89	2.33	1.06	1.82	1.99	0.93	3.02	1.29
Spectral (virtual channels)	Compensated	0.62	1.17	2.20	2.31	0.80	1.07	5.09	1.97	0.97	1.79	2.42	1.11	2.97	1.57
Spectral	Unmixed	0.63	1.07	1.91	2.98	0.76	1.20	1.52	1.38	0.99	2.10	2.83	0.78	2.84	1.20

(K) **Signal resolution**

Conventional	Compensated	25.33	79.20	38.71	20.96	29.15	372.57	11.58	8.58	128.55	290.75	35.82	34.33	10.48	15.99
Spectral (peak channels)	Compensated	26.36	155.60	101.26	42.07	113.77	428.31	12.01	23.43	88.65	263.44	83.11	62.94	18.07	42.49
Spectral (virtual channels)	Compensated	29.53	166.41	97.03	55.52	135.11	441.84	13.82	27.22	103.30	264.27	92.18	63.61	18.02	34.14
Spectral	Unmixed	26.99	134.71	100.52	38.73	129.20	400.39	27.42	45.65	107.77	227.91	96.57	53.30	22.13	52.40

Figure 2. Legend on next page.

many cases, this reduction in spread was paired with an increase in the resolution of blue from red signal (e.g., BV711 vs BV785).

One possible explanation for these differences was that the "peak" detectors used on the spectral system were capturing different light spectra, due to their smaller band pass filter range (e.g., the FITC detector on the conventional system captures 500–550 nm, whereas the "peak" FITC detector on the Aurora captures 498–518 nm). To test this, we compensated data from the spectral system using virtual filters, where data were integrated from multiple detectors to match (as closely as possible) the band-pass filter range of the corresponding detector on the conventional system (Supporting Information Fig. S3). When we compared compensated data from these virtual channels against the compensated peak channel data, or data from the conventional system, we found little change in either spread or resolution values (Fig. 2C,G,J,K).

Spectral Unmixing and Compensation

On many conventional systems, fluorophores with very similar peak emission properties are often captured using the same wide band-pass filter, meaning that only one of those fluorophores may be used in a given panel (e.g., APC and

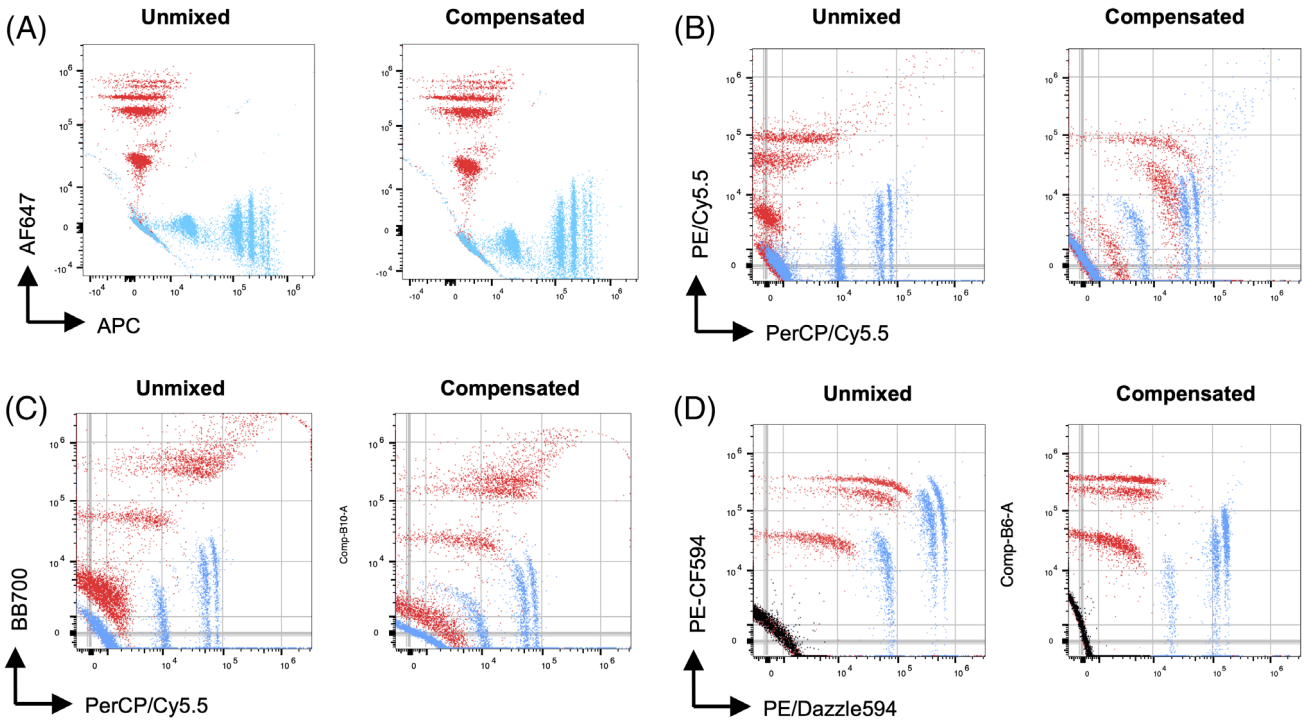

Figure 3. Comparing compensation and spectral unmixing on the spectral system. QSCBs labeled with various fluorophores, subject to spectral unmixing (SpectoFlo) or compensation (FlowJo). Beads were labeled with (**A**) AF647 and APC, (**B**) PE/Cy5.5 and PerCP/Cy5.5, (**C**) BB700 and PerCP/Cy5.5, or (**D**) PE-CF594 and PE/Dazzle594. In some cases, these fluorophores had the same "peak" detector. As such, for compensation, one fluorophore had to be assigned to a nonoptimal channel in order to perform compensation.

Figure 2. Signal comparisons between the conventional and spectral systems. Compensation beads labeled with various fluorophores plotted against each other. For the data in this figure, the fluorophores tested were excited using the same lasers on both the conventional (BD Fortessa X-20) and spectral (Cytek Aurora) systems. Of note, PE-CF594 was detected using the blue laser on both the spectral system and the conventional system, having a Yellow/Green 561 nm option available on the conventional system. The spread of one fluorophore signal (red) is plotted (and measured) against a (**A–D**) neighboring fluorophore (blue) on the same laser, or (**E–H**) another fluorophore (blue) with similar emission properties that is primarily excited by a different laser (cross-laser fluorophore). The degree of spread (red) and the resolution of signal (blue) from spread (red) are quantified by two ratios. Spread is calculated as the 99th percentile of the spreading fluorophore (red) in the receiving detector, divided by the 99th percentile of unstained beads in the same channel. Resolution is calculated as the median of the receiving fluorophore (blue) in the receiving detector, divided by the 99th percentile of the spreading signal (red). Spreading results for fluorophore pairs are provided in **J** (where increasing values are indicated by the intensity of color grading from white to red), and resolution results are provided in **K** (where increasing values are indicated by the intensity of color grading from white to blue). Comparisons were made for: (**A, E**) data from the conventional system when compensated, (**B, F**) data from the spectral system (using "peak" signal detectors only) when compensated, (**C, G**) data from the spectral system (using virtual channels derived from integrated signal) when compensated, and (**D, H**) data from the spectral system when unmixed. Details on the integration of signal into virtual channels are provided in the Supporting Information Figure S3. Red arrows indicate occasions where greater signal spread was observed for data from the conventional system, compared to data from the spectral system.

AF647). A key claim of the spectral approach is that dyes with similar emission properties can be analyzed simultaneously in sufficient detail on a spectral system to create a signature through the use of a larger number of detectors, allowing these signals to be spectrally "unmixed" from each other. However, as these comparisons are often made in the context of unmixing performed on a spectral system and compensation performed on a conventional system, the relative contributions of the system itself (detection methods, optical configurations, detection sensitivity, electronic noise, etc) and the signal correction process (compensation, unmixing) are often intertwined. While a thorough mathematical comparison of the signal correction approaches was outside the scope of this study, it has been studied elsewhere (19). However, in our study, we sought to determine if the *provided* unmixing approach gave any specific advantages over compensation in the context of a spectral analyzer (Fig. 2D,H). Overall, we found that unmixed and compensated data were largely comparable (Fig. 2J,K), where spread and resolution for unmixed data for the fluorophores examined were similar to compensated peak channel or virtual filter data from the spectral system. However, we did find some cases where unmixing led to reduced spread and increased resolution, such as in PE-CF594 vs PerCP/Cy5.5.

Separation of Highly Overlapping Fluorophores Using Spectral Unmixing and Compensation

Despite this, we reasoned that spectral unmixing may result in improvements in signal resolution for fluorophores that had very similar peak emission properties, due to the more detailed spectral signature that can be measured on the Aurora. To test this, we labeled QSCB multilevel capture beads with a variety of fluorophores, including a number of highly overlapping fluorophores that would not normally be combined on a conventional system as they would be measured in the same detector. These samples were recorded on the spectral system and subject to compensation (using FlowJo v10.6.1) or spectral unmixing. For some dyes that are typically measured in the same detector but are spectrally distinct, such as AF647 and APC, we were able to successfully separate these signals using either compensation (peak channel) or spectral unmixing (Fig. 3A), although we did find better resolution in the unmixed data. However, for other dyes with similar emission properties, such as PE/Cy5.5 and PerCP/Cy5.5 (Fig. 3B) or BB700 and PerCP/Cy5.5 (Fig. 3C), we found that we these two signals were substantially better resolved from each other when subject to spectral unmixing, compared with (peak channel) compensation. Nevertheless, we also found some instances where compensation resulted in better signal resolution than unmixing (Fig. 3D).

Comparing Leukocyte Panels on Conventional vs Spectral System

Importantly, we sought to explore the application of spectral cytometry for mid to large size panels from the perspective of a cytometry user and how this technology may apply to their research. Thus, we compared the resolution of cellular populations on the two systems. To do this we labeled bone marrow (BM) cells from mock- or West Nile virus (WNV)-infected mice with a panel of antibodies against typical leukocyte markers. After staining and fixation, each sample was split into two and run in parallel on a conventional system (using four lasers, compensated) and a spectral system (using three lasers, unmixed). Although different lasers were used on each system, we sought to determine if the staining patterns and frequencies of each population were comparable between systems. We adjusted the plots so that a comparable dynamic range was displayed for each system, and the frequencies of each population were calculated.

We examined BM cells from mock-infected animals and compared data generated on the spectral and conventional systems for singlets, cells, live cells, leukocytes (Fig. 4A–D), T cells, NK cells, NKT cells, $CD4^+$ T cells, $CD8\alpha^+$ T cells, plasmacytoid dendritic cells (PDCs), B cells, conventional dendritic cells (cDCs) (Fig. 4E–H), neutrophils, eosinophils, resident macrophages, $Ly6C^{hi}$ monocytes, and $Ly6C^{lo}$ monocytes (Fig. 4I–L). Overall, both the staining patterns and quantification of each of these populations were largely comparable between the two systems (Supporting Information Fig. S4A).

In addition to examining normal BM, we also sought to compare the resolution of each system on a more complex assay that included intranuclear staining. To this end, we designed a seven-color panel identifying regulatory T cells in the murine spleen. As with the BM samples, each sample was split into two and the same panel run in parallel on a conventional system (using four lasers, compensated) and a spectral system (using three lasers, unmixed). In each data set, we examined singlets, cells, live cells (Fig. 5A), T cells (Fig. 5B), $CD4^+$, and $CD8\alpha^+$ T cells (Fig. 5C). Within the $CD4^+$ T-cell population, $FoxP3^+CD25^+$ regulatory T cells were identified (Fig. 5D, left panel), using the fluorescence minus one (FMO) samples to determine the cut-off values for populations (Fig. 5D, center and right panel). Interestingly, we found two prominent differences in this case. The resolution of AF700 CD4 from the spread of BV711 CD8α was improved on the spectral system, as was the resolution of APC FoxP3 from background.

Comparing Brain Samples Panels on Conventional vs Spectral System

We also sought to compare more highly autofluorescent samples. To do this we infected mice with WNV and isolated brain tissue for flow cytometry 7 days post infection. As with the BM, each sample was split into two and the same panel run in parallel on a conventional system (using four lasers, compensated) and a spectral system (using three lasers, unmixed). In each data set, we examined singlets, cells, live cells, leukocytes, (Fig. 6A–D), neutrophils, eosinophils, NK cells, NKT cells, $CD4^+$ T cells, $CD8\alpha^+$ T cells (Fig. 6E–H), PDCs, B cells, cDC, microglia, $Ly6C^{hi}$ and $Ly6C^{lo}$ infiltrating monocytes (Fig. 6I–L). Overall, we found staining patterns and quantification to be similar between the systems (Supporting Information Fig. S4B). However, population

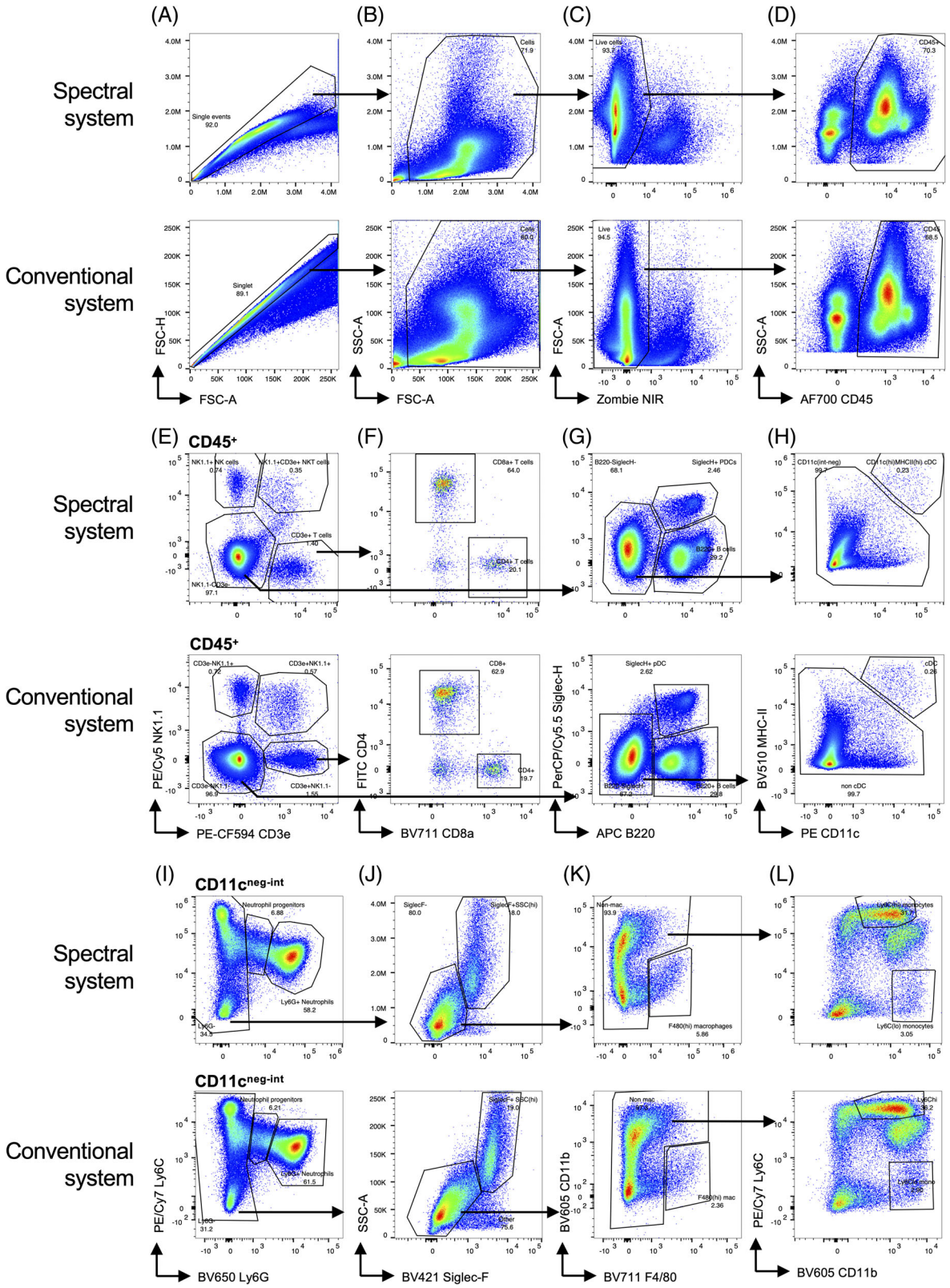

Figure 4. Legend on next page.

resolution in fluorophores being measured in areas of high autofluorescence clearly differed between the samples acquired on the conventional versus spectral system, as described below.

Autofluorescence Extraction

An additional advantage of a spectral approach is in the separate measurement of autofluorescence. By measuring the whole fluorescent spectrum of unstained cells, and treating this fluorescent signature as another fluorophore, the autofluorescent signal can be used as another marker for cellular identification of, for example, neutrophils or senescent cells (21, 22). Alternatively, the autofluorescent signal can be reduced by unmixing the signal from other signals (referred to as extraction), potentially improving resolution in some channels, particularly for cells from highly autofluorescent organs like liver, brain and skin. To determine the extent to which autofluorescence extraction improves resolution, we sought to compare highly autofluorescent samples on both the conventional and spectral systems, including using autofluorescence extraction in the unmixing process for data generated on the Aurora.

The autofluorescence signal in the CNS samples was highest in the 500–650 nm region, in particular in the detectors for the violet laser, but there is also substantial signal measured from the blue laser. By comparing unmixed data, with or without including autofluorescence measured on unstained cells as a parameter, we determined whether autofluorescence extraction improved the resolution of signal in brain samples. In comparing the fluorescence spectrum of the unstained brain to the spectra of the various fluorophores, it is clear that the interference is largest with FITC and BV510 (Fig. 7A). This is also obvious in the labeled samples, with discrimination of individual populations being almost impossible due to autofluorescence interference (Fig. 7B). When autofluorescence extraction was applied, the populations became clear (Fig. 7C), increasing the resolution ratio of the measured populations (defined as the median of the positive population, divided by the 99th percentile of the negative population). BV605 is still in this region where autofluorescence impacts the signal (Fig. 7D), although the interference is much less than with FITC and BV510 (Fig. 7E, F). When examining the spectrum around the 780 nm region (Fig. 7G), autofluorescence makes little difference to the signal in these samples, and thus subtraction of autofluorescence does not substantially improve resolution (Fig. 7H,I).

Discussion

Spectral cytometry provides a number of potential advantages over conventional cytometry through the detailed measurement of the fluorescent spectrum for each fluorophore. In this study, we sought to compare the performance of a spectral cytometry system with conventional system. Overall, the systems were comparable for the applications we tested when performing compensation or spectral unmixing on either system. However, a number of differences between the two approaches were apparent.

Signal Comparability of the Systems

Overall, the resolution of signal from background on the systems was comparable. In comparing signal resolution, we looked at two main factors: signal from background (e.g., the separation between the negative and positive population) and signal spread. The former showed greater resolution of signal from background for the fluorophores on the conventional system, while for the latter we found a decrease in signal spread from measurements made on the spectral system, compared to the conventional system, and in many cases, this was accompanied by an increase in resolution of signal from spread. It is likely that the use of avalanche photodiode (APD) detectors on the spectral system contributes to the improved resolution of some of these signals, compared to the photomultiplier tube (PMT) detectors used on the conventional system, as APD have been shown to perform better in spectral regions over 650 nm due to increased sensitivity in these parts of the spectrum (23). Importantly, although the resolution of individual signals from background was lower on the spectral system compared to the conventional system in this comparison, the improved signal resolution from signal spread in most cases indicates better performance in a mixed panel context. Of note, in our comparison, we used two conventional cytometers with specific configurations, and as such, these comparisons may differ for other conventional cytometers.

Spectral Unmixing vs Compensation

Importantly, spectral unmixing did not eliminate spreading error, despite increased signal resolution from spreading error in many cases. However, fluorophores that are very similar

Figure 4. Instrument comparison using a general leukocyte panel on bone marrow cells. Bone marrow cells were stained with a general immune panel and run on the three-laser spectral system or a four-laser conventional system. On the spectral system, PE and PE tandem fluorophores were excited with the blue laser, and on the conventional system, they were excited using the Yellow/Green 561 nm laser. Samples were gated for (**A**) singlets, (**B**) cells, (**C**) live cells, and (**D**) $CD45^+$ leukocytes. (**E**) T cells ($CD3\varepsilon^+NK1.1^-$), NKT cells ($CD3\varepsilon^+NK1.1^+$), and NK cells ($CD3\varepsilon^-NK1.1^+$) were gated, and (**F**) T cells were further subdivided into $CD4^+$ and $CD8\alpha^+$ subsets. (**G**) $CD3\varepsilon^-NK1.1^-$ cells were gated for B cells ($B220^+$Siglec-H^-) and PDCs ($B220^+$Siglec-H^+), and (**H**) $B220^-$Siglec-H^- cells were then gated for $CD11c^{hi}$MHC-II^{hi} cDCs. (**I**) $CD11c^{neg\text{-}int}$MHC-$II^{neg\text{-}int}$ cells were then gated for mature ($Ly6G^{hi}$) and immature ($Ly6G^{int}$) neutrophils, and (**J**) $Ly6G^-$ cells were then gated for Siglec-F^+ eosinophils. (**K**) Siglec-F^- cells were then gated for $F4/80^+$ macrophages and (**L**) $Ly6C^{hi}CD11b^+$ monocytes. The plot axes were adjusted so that dynamic range could be directly compared between each system.

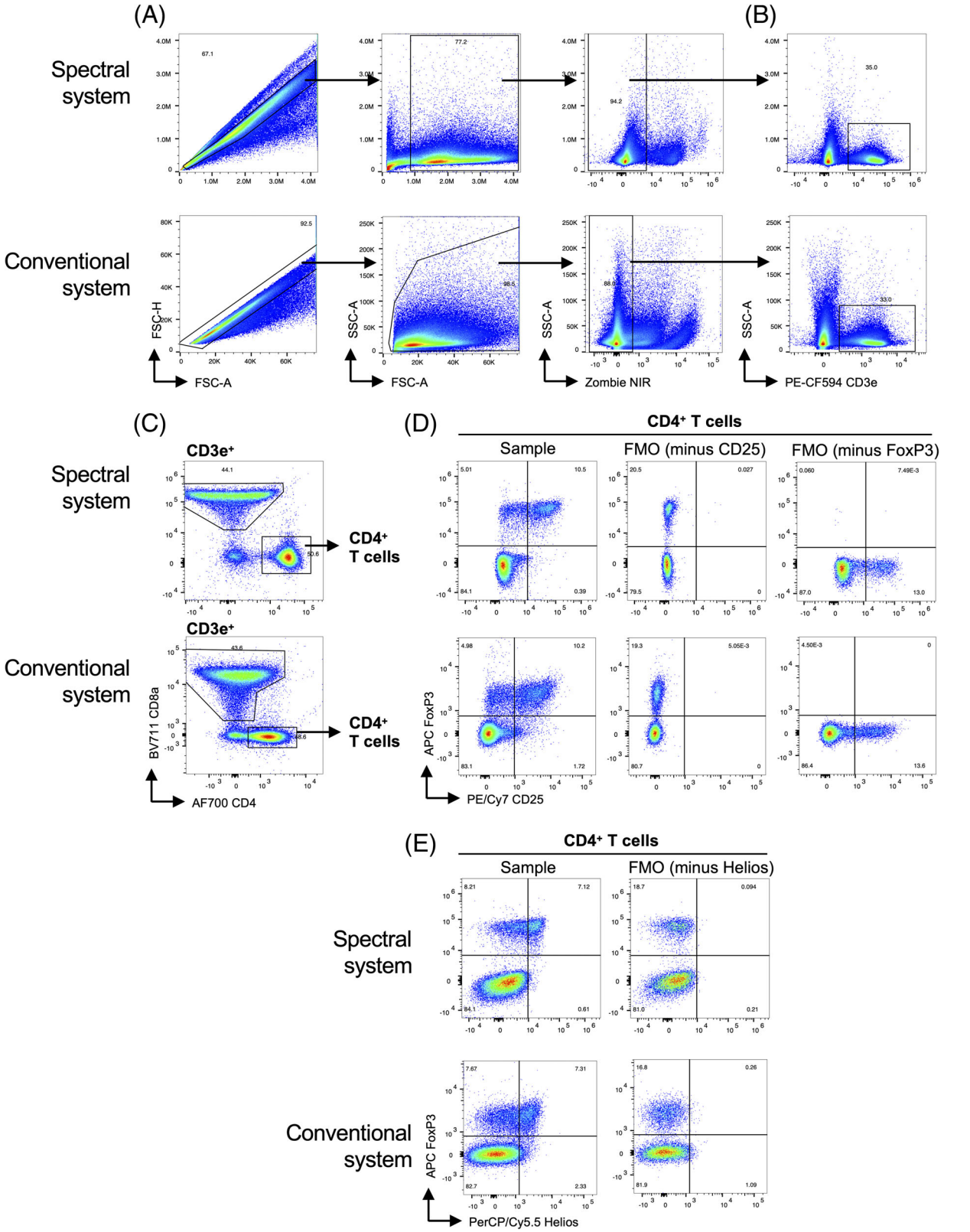

Figure 5. Instrument comparison using a T-cell panel on spleen cells. Samples acquired on a three-laser spectral system or five-laser conventional system. On the spectral system, PE and PE tandem fluorophores were excited with the blue laser, and on the conventional system they were excited using the Yellow/Green 561 nm laser. Samples were gated for (**A**) singlets, cells, live cells. (**B**) Samples were then gated for CD3ε$^+$ cells, which were then further subdivided into (**C**) CD4$^+$ and CD8α$^+$ subsets. T-cell subsets where then gated for various combinations of (**D**, **E**) FoxP3, CD25, and Helios, using fluorescence minus one (FMO) controls to guide the placement of gates. The plot axes were adjusted so that dynamic range could be directly compared between each system.

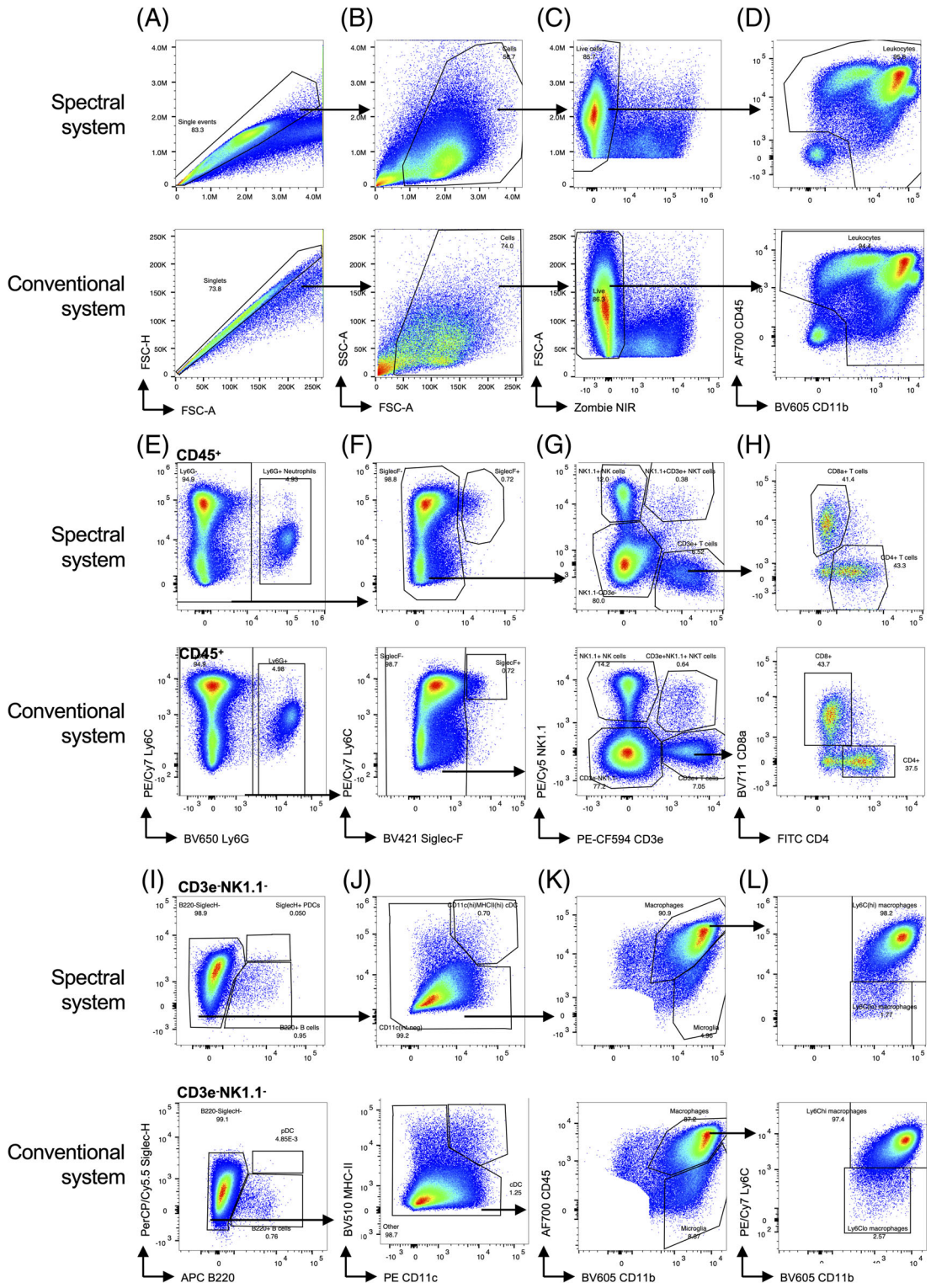

Figure 6. Instrument comparison using a general leukocyte panel on cells isolated from infected murine brains. WNV-infected murine brain samples were run on the three-laser spectral system or four-laser conventional system. On the spectral system, PE and PE tandem fluorophores were excited with the blue laser, and on the conventional system they were excited using the Yellow/Green 561 nm laser. Samples were gated for (**A**) singlets, (**B**) cells, (**C**) live cells, and (**D**) $CD45^+$ leukocytes. (**E**) $Ly6G^+$ neutrophils and (**F**) Siglec-F^+ eosinophils were gated, before gating (**G**) T cells ($CD3\varepsilon^+NK1.1^-$), NKT cells ($CD3\varepsilon^+NK1.1^+$), and NK cells ($CD3\varepsilon^-NK1.1^+$). (**H**) T cells were further subdivided into $CD4^+$ and $CD8\alpha^+$ subsets. (**I**) $CD3\varepsilon^-NK1.1^-$ cells were gated for B cells ($B220^+$Siglec-H^-) and PDCs ($B220^+$Siglec-H^+), and (H) $B220^-$Siglec-H^- cells were then gated for $CD11c^{hi}$MHC-II^{hi} cDCs. (**K**) Cells were then gated for $CD45^+CD11b^+$ infiltrating myeloid cells, and $CD45^{lo}CD11b^+$ microglia. (**L**) $CD45^+CD11b^+$ cells were then gated for $Ly6C^{hi}CD11b^+$ infiltrating monocyte-derived macrophages. The plot axes were adjusted so that dynamic range could be directly compared between each system.

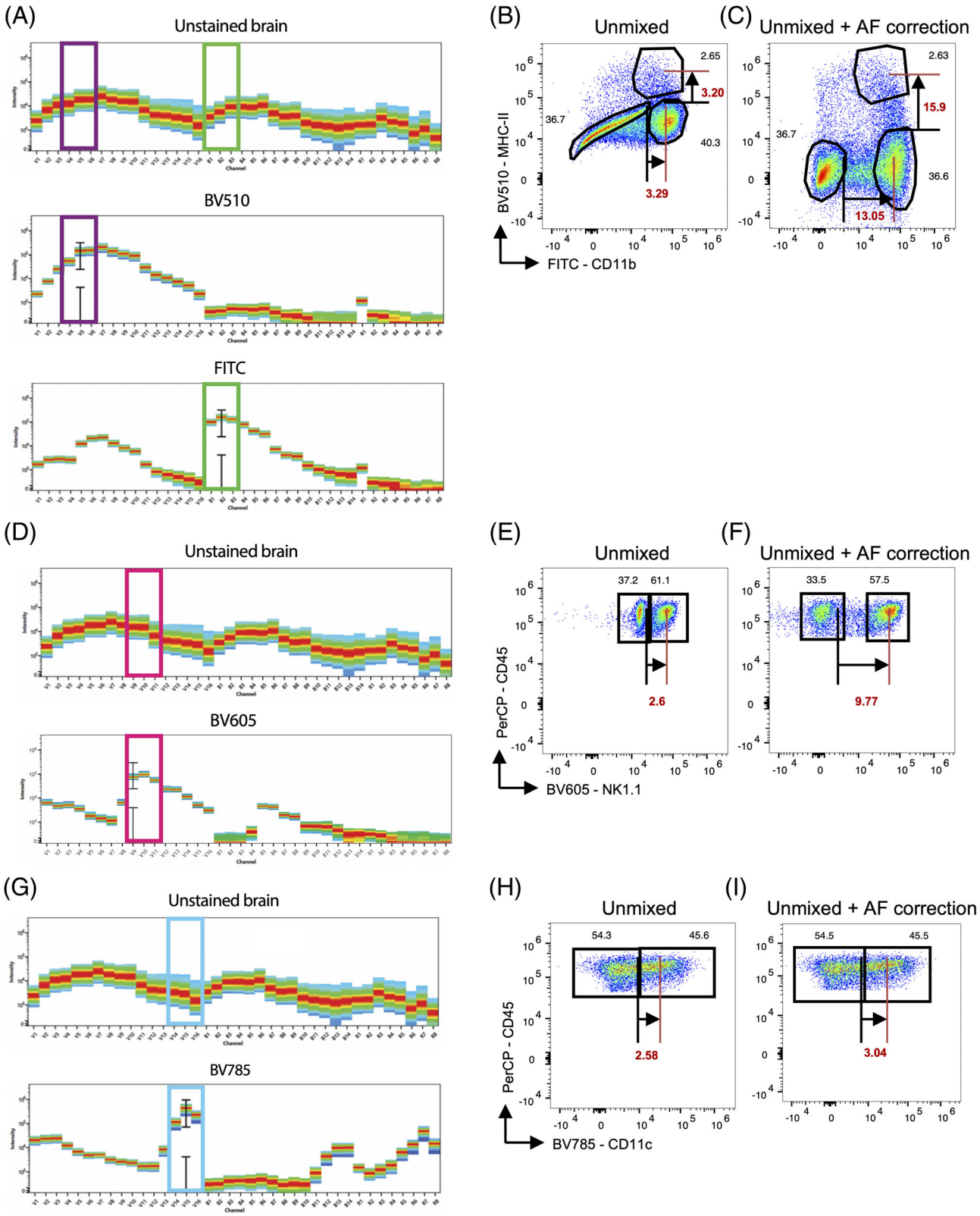

Figure 7. Legend on next page.

may gain an additional resolution from the measurement of the complete spectrum of each, enabling more accurate discrimination between them than can be achieved using compensation. This was observed for a number of highly overlapping fluorophores that we tested. However, in one comparison, (PE-CF594 vs PE/Dazzle594) compensation appeared to result in improved resolution over unmixing. It is possible that optimizing the use of specific channels on the spectral system could maximize the level of signal of target fluorophore relative to the spillover fluorophore being detected. In this case, compensated data might be able to separate the signals in a manner similar to unmixing. However, attempting to optimize this is time consuming, and in many cases, applying the unmixing approach appears to result in satisfactory results compared with compensation.

Autofluorescence Extraction during Spectral Unmixing Increases Population Resolution in Autofluorescence Wavelength Ranges

A key advantage in performing spectral unmixing is the measurement and extraction of cellular autofluorescence in labeled cells. In regions of the spectrum that exhibit low cellular autofluorescence, or in cells that exhibit low autofluorescence, this is of little advantage. However, in autofluorescent cells, in spectral regions where high levels of cellular autofluorescence are observed, such as around the 500–600 nm region, autofluorescence extraction markedly improved the resolution of populations. This is a critical advantage applicable to a wide range of biological contexts, especially where autofluorescence impedes the use of a large number of fluorophores on certain cell types or tissues, as well as where the measurement of autofluorescence as an additional parameter may yield interesting biological insights.

The Spectral Approach Allows for Far Greater Flexibility in Fluorophore Choice and Panel Design

A key component of panel design in conventional cytometry, is the choice of fluorophores that are able to be detected on a given system, considering the excitation lasers and optical filters available. For example, in our conventional system, the red laser has three associated detectors, with filters designed to capture APC (or AF647), AF700, and APC/Cy7 (or APC/H7), respectively. An outcome of using a larger number of detectors in the spectral system is greater flexibility afforded in the approach to panel design. This was most evident when fluorophores were used together that would normally occupy the same detector on a conventional system (e.g., APC, AF647). However, this is also relevant for fluorophores that are less overlapping, but when used in conventional cytometers, the choice of one or the other has to be made, for example, PerCP and PerCP/Cy5.5. As such, approaches to panel design need not begin with a review of which fluorophores are compatible with the instrument (based on the available filters), but rather a consideration of which possible combinations of fluorophores can be successfully resolved from one another. This allows selection from a wider range of fluorophores, rather than a limited list of instrument-compatible fluorophores.

The Role of Spectral Cytometry among Conventional High-Dimensional Fluorescence and Mass Cytometry

In the field of single-cell science, the techniques of (conventional) flow cytometry, mass cytometry, image cytometry, and genomic cytometry (single-cell RNA sequencing and associated oligonucleotide reporters for antibody labeling (24)), have all developed their own strengths and weaknesses. Flow cytometry provides a high-throughput and cost-effective method of measuring few parameters (currently up to approx. 27 fluorophores published, with up to 40 fluorophores reported) on many cells with high-throughput (approx. 10,000 events/s). Mass cytometry, on the other hand, acquires cells at a much lower rate (approx. 300–400 events/s), but with more markers per cell (over 50 metals), with significantly reduced overlap between reporters. Single-cell sequencing measures cells at a very low throughput and high cost, but it is capable of measuring hundreds to thousands of genes per cell (RNA, transcriptome), and more recently has incorporated oligonucleotide-based reporters for antibody labeling of cells (proteome/epitome) (24), as well as epigenomic and other single cell measurements (25, 26). Ignoring cost, these technologies represent a spectrum between greater numbers of cells with fewer features per cell, and fewer cells with more features per cell per unit time. Spectral cytometry potentially improves on conventional flow cytometry by enabling the use of previously impracticable fluorophore series, thereby also providing increased flexibility of panel design, as well as incorporating autofluorescence measurement and extraction.

In contrast to the use of fluorescent molecules in flow cytometry, mass cytometry uses heavy metal tags and time-of-flight mass spectrometry readouts to measure antibody binding to cells. This method allows a much larger number of simultaneous markers than conventional flow cytometry. However, while mass cytometry is often used for rare and precious samples, the time investment in acquiring samples and performing analysis is higher than for flow cytometry. Thus, for researchers seeking to acquire and analyze data quickly, but requiring more colors than are available on conventional instruments, spectral cytometry provides a potential opportunity. Moreover, the use of the same fluorophore-

Figure 7. Autofluorescence correction performed on WNV-infected brain cells. (**A**) Spectral signatures generated on the spectral system for unstained cells, BV510-labeled beads, and FITC-labeled beads. Fully stained samples unmixed on the spectral system (**B**) without and (**C**) with autofluorescence correction. (**D**) Spectral signatures generated on the spectral system for unstained cells and BV605-labeled beads. Fully stained samples unmixed on the spectral system (E) without and (**F**) with autofluorescence correction. (**G**) Spectral signatures generated on the spectral system for unstained cells and BV785-labeled beads. Fully stained samples unmixed on the spectral system (**H**) without and (**I**) with autofluorescence correction for BV785-CD11c. For each plot, percentages of cells in each populations are show, as well a resolution ratio for each population, defined as the median of the positive population, divided by the 99th percentile of the negative population.

conjugated antibodies, staining, and analysis techniques as conventional cytometry make this a well-characterized, readily accessible technique, while also allowing an increased number of markers to be measured. Additionally, researchers using smaller panels may benefit from the flexibility of the system, with a larger range of fluorophores being compatible with the system, aiding panel design.

While spectral approaches to fluorescence cytometry have been developed for some time, spectral cytometry is an emerging technology in the commercial space and is still maturing. However, the nature of the spectral approach exhibits several clear advantages over conventional cytometry and should be incorporated into routine cytometry approaches where possible.

Acknowledgments

Thomas Ashhurst is supported by the International Society for the Advancement of Cytometry (ISAC) Marylou Ingram Scholars Program. Paula Niewold is supported by the International Society for the Advancement of Cytometry (ISAC) Marylou Ingram Scholars Program. This work was supported by National Health and Medical Research Council Project Grant 1088242 and a grant from the Merridew Foundation.

Author Contributions

Paula Niewold: Conceptualization-Lead, Data curation-Equal, Formal analysis-Equal, Investigation-Equal, Methodology-Equal, Project administration-Lead, Software-Equal, Supervision-Equal, Validation-Equal, Visualization-Equal, Writing-original draft-Lead, Writing-review & editing-Equal. **Thomas Ashhurst:** Conceptualization-Equal, Data curation-Equal, Formal analysis-Equal, Investigation-Equal, Methodology-Equal, Software-Equal, Validation-Equal, Visualization-Equal, Writing-original draft-Equal, Writing-review & editing-Equal. **Adrian Smith:** Conceptualization-Equal, Formal analysis-Supporting, Investigation-Supporting, Methodology-Supporting, Resources-Equal, Supervision-Equal, Writing-review & editing-Supporting. **Nicholas King:** Conceptualization-Supporting, Funding acquisition-Lead, Investigation-Supporting, Methodology-Supporting, Project administration-Supporting, Resources-Equal, Supervision-Equal, Writing-original draft-Supporting, Writing-review & editing-Equal.

Literature Cited

1. Roederer M. Spectral compensation for flow cytometry: Visualization artifacts, limitations, and caveats. Cytometry 2001;45(3):194–205.
2. Roederer M. Compensation in flow cytometry. Curr Protoc Cytom 2002;22: 1.14.1–1.14.20. https://doi.org/10.1002/0471142956.cy0114s22
3. Bagwell CB, Adams EG. Fluorescence spectral overlap compensation for any number of flow cytometry parameters. Ann N Y Acad Sci 1993;677:167–184.
4. Nguyen R, Perfetto, S, Mahnke, YD, Chattopadhyay, P, Roederer, M. Quantifying spillover spreading for comparing instrument performance and aiding in multicolor panel design. Cytom Part A 2013;83A(3):306–315.
5. Ashhurst TM, Smith AL, King NJC. High-dimensional fluorescence cytometry. Curr Protoc Immunol 2017;119:5 8 1–5 8 38.
6. Mair F, Prlic M. OMIP-44: 28-color immunophenotyping of the human dendritic cell compartment. Cytometry A 2019;95A(8):925–926.
7. Nettey L, Giles AJ, Chattopadhyay PK. OMIP-050: A 28-color/30-parameter fluorescence flow cytometry panel to enumerate and characterize cells expressing a wide Array of immune checkpoint molecules. Cytometry A 2018;93A(11):1094–1096.
8. Robinson J, Rajaw B, Gregori G, Jones J, Patsekine V. Collection hardware for high speed multispectral single particle analysis. Congress of the International Society for Analytical Cytology 2004; p. 12.
9. Robinson J. Multispectral cytometry: The next generation. Biophoton Int 2004;8: 36–40.
10. Robinson JP, Rajwa B, Gregori G, Patsekin. Multispectral Detector and Analysis System. 2007; Purdue University, US patent 72,802,042,007.
11. Robinson JP. Spectral flow cytometry-Quo vadimus? Cytom Part A 2019;95A(8): 823–824.
12. Nolan JP, Duggan E, Liu E, Condello D, Dave I, Stoner SA. Single cell analysis using surface enhanced Raman scattering (SERS) tags. Methods 2012;57(3):272–279.
13. Nolan JP, Condello D. Spectral flow cytometry. Cur Protoc Cytom 2013;63(1):27. http://dx.doi.org/10.1002/0471142956.cy0127s63.
14. Nolan JP et al. Visible and near infrared fluorescence spectral flow cytometry. Cytom Part A 2013;83A(3):253–264.
15. Futamura K, Sekino M, Hata A, Ikebuchi R, Nakanishi Y, Egawa G, Kabashima K, Watanabe T, Furuki M, Tomura M. Novel full-spectral flow cytometry with multiple spectrally-adjacent fluorescent proteins and fluorochromes and visualization of in vivo cellular movement. Cytom Part A 2015;87A(9):830–842.
16. Schmutz S, Valente M, Cumano A, Novault S. Spectral cytometry has unique properties allowing multicolor analysis of cell suspensions isolated from solid tissues. PLoS One 2016;11(8):e0159961.
17. Park LM, Lannigan J, Jaimes, MC. OMIP-069: Forty-Color Full Spectrum Flow Cytometry Panel for Deep Immunophenotyping of Major Cell Subsets in Human Peripheral Blood. Cytometry Part A. 2020. https://doi.org/10.1002/cyto.a.24213.
18. Zimmermann T. Spectral imaging and linear unmixing in light microscopy. Adv Biochem Eng Biotechnol 2005;95:245–265.
19. Novo D, Gregori G, Rajwa B. Generalized unmixing model for multispectral flow cytometry utilizing nonsquare compensation matrices. Cytom A 2013;83A(5): 508–520.
20. Ashhurst TM, Cox DA, Smith Al, King NJC. Analysis of the bone marrow haematopoietic system using mass and flow cytometry. In: McGuire HM, Ashhurst TM, editors. Protocols in Mass Cytometry, Methods in Molecular Biology, New York, NY: Springer, 2019.
21. Dorward DA, Lucas CD, Alessandri AL, Marwick JA, Rossi F, Dransfield I, Haslett C, Dhaliwal K, Rossi AG. Technical advance: Autofluorescence-based sorting: Rapid and nonperturbing isolation of ultrapure neutrophils to determine cytokine production. J Leukoc Biol 2013;94(1):193–202.
22. Bertolo A, Baur M, Guerrero J, Pötzel T, Stoyanov J. Autofluorescence is a reliable in vitro marker of cellular senescence in human mesenchymal stromal cells. Sci Rep 2019;9(1):2074.
23. Lawrence WG, Varadi G, Entine G, Podniesinski E, Wallace PK. A comparison of avalanche photodiode and photomultiplier tube detectors for flow cytometry. SPIE BiOS 2008;6859. https://doi.org/10.1117/12.758958.
24. Stoeckius M, Hafemeister C, Stephenson W, Houck-Loomis B, Chattopadhyay PK, Swerdlow H, Satija R, Smibert P. Simultaneous epitope and transcriptome measurement in single cells. Nat Methods 2017;14(9):865–868.
25. Hu Y, Huang K, An Q, Guizhen D, Hu G, Xue J, Zhu X, Wang C, Xue Z, Fan G. Simultaneous profiling of transcriptome and DNA methylome from a single cell. Genome Biol 2016;17:88.
26. Mimitou E, Cheng A, Montalbano A, Hao S, Stoeckius M, Legut M, Roush T, Herrera A, Papalexi E, Ouyang Z, et al. Expanding the CITE-seq tool-kit: Detection of proteins, transcriptomes, clonotypes and CRISPR perturbations with multiplexing, in a single assay. Nat Methods 2018:16(5):409–412.